Original Article

Institution of MECHANICAL ENGINEERS
Journal of AEROSPACE ENGINEERING

Proc IMechE Part G:
J Aerospace Engineering
0(0) 1–11

DOI: 10.1177/0954410018823623
journals.sagepub.com/home/pig
SAGE

Opto-electronic platform tracking control of multi-rotor unmanned aerial vehicles based on composite disturbance compensation

Rijun Wang[1], Yue Bai[2], Zhiqiang Zeng[1], Junyuan Wang[1], Wenhua Du[1] and Nengquan Duan[1]

Abstract

Airborne opto-electronic platforms are very important in unmanned aerial vehicle systems. The stability and tracking performance of airborne opto-electronic platforms are easily affected by disturbance factors, making compensating for those disturbances a very prominent issue. In this paper, compared to the traditional disturbance observer, an improved velocity signal based disturbance observer (IVDOB) is particularly designed to compensate for the disturbance. Then its capability, robustness, and stability are discussed. For improving the stabilization accuracy and tracking performance of airborne opto-electronic platforms, the universal approximation property of fuzzy systems is used to compensate the disturbance further and an adaptive fuzzy control system based on IVDOBs is proposed. To validate the scheme, a series of experiments were carried out. The results show that the proposed control scheme can achieve reliable control precision and satisfy the requirements of airborne opto-electronic platform tasks.

Keywords

Multi-rotor unmanned aerial vehicle, airborne opto-electronic platform, composite disturbance compensation, disturbance observer, approximation property

Date received: 22 May 2018; accepted: 13 December 2018

Introduction

The multi-rotor unmanned aerial vehicle (mUAV) is an important branch of unmanned aerial vehicles and is better adaptable to the environment. It can fly forward, inverted, hover, and so on. It has the independent cruise flight ability and autonomous landing capabilities. Therefore, the mUAV has broad application prospects and development prospects in military and civilian fields.[1–3]

The opto-electronic platform system mounted on mUAVs improves the control precision of the aircraft while extending the aircraft vision ability as well. It is the key to the application of reconnaissance, mapping, tracking, and other fields. The importance of the airborne opto-electronic platform (AOEP) is obvious.[4] However, the mUAV has the advantages of being light in weight, small in volume, and having a low lift to weight ratio, which causes the stability of the AOEP to be easily affected by disturbance factors such as airframe attitude change, airflow, mechanical vibration, moment coupling, and other unknown disturbances. Those disturbance factors have the characteristics of a large range of frequency distributions, large amplitude variations, nonlinearity, and strong coupling.[5] Due to the existence of the above disturbance factors, the airborne video and image obtained by the ground station can be jittery, blurred, defocused, and with even possibilities of the target disappearing from the field of view. It is easy for the operator's visual fatigue to lead to the wrong operation when even they cannot identify the target clearly. This would seriously lead to the inability to complete reconnaissance, mapping, tracking, and other tasks.

Since the development of mUAV was not too long ago, the mechanisms of the disturbance factors are not clear and the related technology accumulation

[1]School of Mechanical Engineering, North University of China, Taiyuan, China
[2]Changchun Institute of Optics, Fine Mechanics and Physics, Chinese Academy of China, Changchun, China

Corresponding author:
Rijun Wang, No. 3, Xueyuan Road, Shanxi, Taiyuan 030051, China.
Email: wangrijun1982@126.com

and engineering practices are even more unclear. The research work on disturbance compensation for AOEPs is full of challenges, but the work is also necessary.[6] The disturbance observer (DOB) proposed by Umeno et al.[7] has the advantages of disturbance compensation ability, lower computational complexity, and no external sensors. The existing disturbance compensation method has been applied widely to compensate for disturbances to the airborne inertial stabilization platform.[8–13] The basic principle of the DOB is using the difference between the output of the actual object and the reconstructed model (or nominal model) as an equivalent disturbance. The difference is the change of the model parameters which are caused by the external disturbance. The equivalent disturbance is used to compensate for the disturbance to the system.[14] The DOB is usually used as the control inner loop to improve the disturbance rejection ability of the system.[15] For DOBs based on velocity, the input signal of the speed loop and the speed output of the control system are used as the inputs and the observed value of the practical disturbance is used as the output.[16] For DOBs based on position, the input signal of the speed loop and the position output of the control system are used as the inputs and the observed value of the practical disturbance is used as the output.[17,18] To some extent, the DOB improves the ability of AOEPs to reduce the disturbance.[19–21] However, the traditional compensation control system based on DOBs is not ideal for the measurement of noise interference and many studies have not considered the influence of the measurement noise on the performance of the system. In some cases of high precision tracking, positioning, precision instrument control, and other high-precision control occasions, the impact of the measurement noise interference cannot be ignored, as the measurement noise interference is a major factor that reduces the control accuracy.[22]

Generally, the disturbance on AOEPs is strongly nonlinear and coupled. Therefore, it is difficult to obtain an ideal control effect by only using a DOB.[23] Intelligent control strategies such as neural networks and fuzzy systems, which have good robustness, do not depend on the system model. Thus, by using the advantages of the approximation properties of any function, these intelligent control strategies are widely used in the servo stabilized platform tracking control system, with better control effect being achieved.[24–28] In order to improve the disturbance rejection ability of the AOEP control system, Wang et al.[29] constructed a hybrid control method based on the adaptive fuzzy grey predictive control. Aiming at the disturbance compensation and the tracking control requirements of AOEPs, the approximation property of fuzzy systems was used together with a DOB to reject the disturbance and the fuzzy adaptive tracking control structure based on the improved DOB was studied.[30] In the compensation control systems of AOEPs, neural networks are also used to compensate for the disturbance and uncertainty of the system. Fang et al.[31] used neural networks to compensate for disturbance and proposed an adaptive decoupling control based on neural networks. The results showed that the stable tracking performance of the three-axis gyro-stabilized platform is improved. Hu et al.[32] used an RBF neural network to approximate the disturbance function of servo tracking control systems. The tracking control structure based on an RBF neural network was constructed and the effectiveness of the method was verified by a three-axis stability test platform.

In this paper, the disturbance compensation and tracking control requirements for the AOEP are discussed. A novel method based on the idea of composite disturbance compensation is proposed. First, an improved DOB based on the velocity signal is proposed to improve the disturbance compensation ability of the DOB. Second, an adaptive fuzzy system is used to estimate the unknown nonlinear disturbance to further enhance the accuracy of the airborne platform stability and to guarantee the stability and tracking performance of the AOEP system.

The remainder of this paper is organized in the following manner. In the next section, the model of the AOEP is established, including the state space model of the AOEP and the actuator dynamic model. Then, an improved velocity signal based DOB is discussed. Next, an adaptive fuzzy control system based on the improved velocity signal based DOB is proposed. Finally, real-time experimental results of the application of the proposed controller to a 3-axis AOEP mounted on a mUAV are presented.

The AOEP system model

The state space model of an AOEP

The AOEP is assumed to be a rigid body; the nonlinear model of the AOEP can be obtained by the Euler-Lagrange equation.[33] Without considering the external disturbance, the nonlinear model can be described as

$$u = M(\theta)\ddot{\theta} + C(\theta, \dot{\theta})\dot{\theta} + F(\dot{\theta}) + g(\alpha) \tag{1}$$

where u (torque) is control input, θ is the feedback of position, $M(\theta)$ is the symmetric inertia matrix, $C(\theta, \dot{\theta})$ is the centrifugal force and the Coriolis forces, $F(\theta)$ is the viscous friction, and $g(\alpha)$ represents a component of gravity. Here α is angle between the arm length and force. The structure of AOEP is designed with carbon fiber which is very light in weight, thus the term $g(\alpha)$ can be ignored.

Assuming the AOEP is rigid, the center of rotation coincides with the center of mass and the term $C(\theta, \dot{\theta})$ can be ignored. Here, the nonlinear model of an

AOEP consistent with the single joint mechanical model can be described as

$$u = J_{eff}\ddot{\theta} + F_v\dot{\theta} + F_c\text{sgn}(\dot{\theta}) \tag{2}$$

where J_{eff} is the effective inertia of the load and F_c is the static friction force. The J_{eff} is obtained by the following formula[34]

$$J_{eff} = \frac{J_a + J_m}{n} + nJ_L \tag{3}$$

where J_a is the inertia of actuator, J_m is the gear inertia, J_L is the inertia of load, and n is the gear ratio.

Substituting equation (3) into equation (2), we get

$$u = \left(\frac{J_a + J_m}{n} + nJ_L\right)\ddot{\theta} + F_v\dot{\theta} + F_c\text{sgn}(\dot{\theta}) \tag{4}$$

In order to facilitate the design of the AOEP control system, the influence of static friction is ignored and the linear model is given as

$$u = J_{eff}\ddot{\theta} + F_v\dot{\theta} \tag{5}$$

Introducing the spatial state variables: $x_1 = \theta$ and $x_2 = \dot{\theta}$, we get the state space equation as follows

$$\begin{cases} \dot{x}_1 = x_2 \\ \dot{x}_2 = -\frac{F_v}{J_{eff}}x_2 + \frac{u}{J_{eff}} \end{cases} \tag{6}$$

The state equation of the AOEP is given as

$$\begin{aligned} \dot{\mathbf{x}} &= \begin{bmatrix} 0 & 1 \\ 0 & -\frac{F_v}{J_{eff}} \end{bmatrix}\mathbf{x} + \begin{bmatrix} 0 \\ \frac{1}{J_{eff}} \end{bmatrix}\mathbf{u} \\ y &= \begin{bmatrix} 1 & 0 \end{bmatrix}\mathbf{x} \end{aligned} \tag{7}$$

that is

$$\begin{cases} \dot{\mathbf{x}} = \mathbf{A}\mathbf{x} + \mathbf{B}\mathbf{u} \\ y = \mathbf{C}x \end{cases} \tag{8}$$

where $\mathbf{x} = \begin{bmatrix} x_1 \\ x_2 \end{bmatrix}$, $\mathbf{A} = \begin{bmatrix} 0 & 1 \\ 0 & -\frac{F_v}{J_{eff}} \end{bmatrix}$, $\mathbf{B} = \begin{bmatrix} 0 \\ \frac{1}{J_{eff}} \end{bmatrix}$, $\mathbf{C} = \begin{bmatrix} 1 & 0 \end{bmatrix}$, $\mathbf{u} = \begin{bmatrix} 0 \\ u \end{bmatrix}$.

Considering the presence of internal disturbance $\boldsymbol{T}_d$, the state space model of the AOEP can be expressed as

$$\begin{cases} \dot{\mathbf{x}} = \mathbf{A}\mathbf{x} + \mathbf{B}u + \boldsymbol{T}_d \\ y = \mathbf{C}x \end{cases} \tag{9}$$

where $\boldsymbol{T}_d = \begin{bmatrix} 0 & -\frac{T_f}{J_{eff}} \end{bmatrix}^{\mathrm{T}}$, T_f is a disturbance term including modeling uncertainties and other internal disturbances. If the coefficients J_{eff} and F_v are known, the state space equation can be solved.

The actuator dynamic model

According to the requirements of the low speed and large torque of AOEPs, a DC torque motor is used in this system. The actuator consists of a DC torque motor with a drive and a rotating shaft. For an actual system, the dynamic equation of the actuator can be rewritten as

$$a_1\ddot{\theta} + a_2\dot{\theta} + u_{\text{d}} = u_o \tag{10}$$

where u_d is the disturbance of actuator and u_o is the output control voltage.

In general, parameters a_1 and a_2 vary with the external environment changes. If we let $a_1 = \hat{a}_1 + \delta a_1$, $a_2 = \hat{a}_2 + \delta a_2$, where $\hat{a}_1$ and $\hat{a}_2$ are the estimated values of a_1 and a_2, they can be obtained by the frequency sweeping method. δa_1 and δa_2 are the perturbations of the variables, thus defining the nonlinear unknown disturbance function as: $f(\theta, \dot{\theta}, \ddot{\theta}) = \delta a_1\ddot{\theta} + \delta a_2\dot{\theta} + u_{\text{d}}$. This includes modeling errors, parameters fluctuation, external perturbations, and so on. Then, the dynamic equation of the actuator can be described as

$$\hat{a}_1\ddot{\theta} + +\hat{a}_2\dot{\theta} + f(\theta, \dot{\theta}, \ddot{\theta}) = u_o \tag{11}$$

The improved velocity-based disturbance observer

The structure of velocity signal-based disturbance observer (VDOB) is shown in Figure 1.

In fact, the external disturbances and the noise disturbances are usually in different frequency ranges. Thus, we can have the following assumptions.

Assumption 1. There are two cut-off frequencies: ω_h and ω_l, where $\omega_l < \omega_h$. The noise disturbances in the high-frequency range are described as $\xi(j\omega) \in (\omega_h, \infty)$. The reference input and external disturbances in the

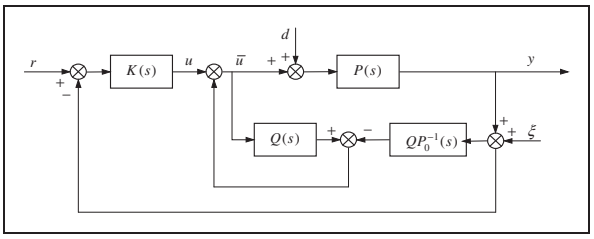

Figure 1. The VDOB-based control system structure. $P(s)$ is the complex field form of the AOEP model as described in equation (9). $P_0(s)$ is the nominal model. r,d, and ξ are the reference input, the external disturbances, and the noise disturbances, respectively.

low-frequency range are described as $d(j\omega) \in (0, \omega_l)$ and $r(j\omega) \in (0, \omega_l)$.

Assumption 2. In the low-frequency range $(0, \omega_l)$, $Q(s) \approx 1$. In the high-frequency range (ω_h, ∞), $Q(s) \approx 0$.

According to Figure 1, the transfer function of the system is described as

$$\begin{aligned} y(s) = & \frac{PP_0K}{PP_0K + P_0 + (P - P_0)Q} r(s) \\ & + \frac{PP_0(1 - Q)}{PP_0K + P_0 + (P - P_0)Q} d(s) \\ & - \frac{P(Q + KP_0)}{PP_0K + P_0 + (P - P_0)Q} \xi(s) \end{aligned} \tag{12}$$

If assumption 2 is established, then the output of the system can be approximately expressed as

$$y(j\omega) \approx \frac{P_0K}{1 + P_0K} r(j\omega), \quad \omega \in (0, \omega_l) \tag{13}$$

$$y(j\omega) \approx -\frac{P_0K}{1 + P_0K} \xi(j\omega), \quad \omega \in (\omega_h, \infty) \tag{14}$$

It can be seen that the control structure based on the VDOB can eliminate the influence of external disturbances completely, but the suppression of the high-frequency noise is not ideal. Focusing on this problem, an improved velocity-based disturbance observer (IVDOB) is proposed. The structure of the IVDOB is shown in Figure 2.

Compared with the VDOB, a compensation controller $Q_2(s)$ is used to compensate the high-frequency disturbances. According to Figure 2, the transfer function of the system is described by

$$\begin{aligned} y(s) = & \frac{PK}{PK + 1 + (P - P_0)(Q_1 - KQ_2)} r(s) \\ & + \frac{1 - P_0Q_1 + KP_0Q_2}{PK + 1 + (P - P_0)(Q_1 - KQ_2)} d(s) \\ & - \frac{PK + PQ_1 - PKQ_2}{PK + 1 + (P - P_0)(Q_1 - KQ_2)} \xi(s) \end{aligned} \tag{15}$$

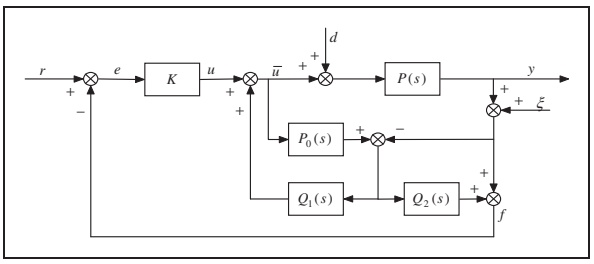

Figure 2. The IVDOB-based control system structure.

In order to compensate for the external disturbances d and the noise disturbances ξ, $Q_1(s)$ and $Q_2(s)$ need to meet the following two conditions

$$1 - P_0Q_1 + KP_0Q_2 \approx 0, \quad \omega \in (0, \omega_l) \tag{16}$$

$$K + Q_1 - KQ_2 \approx 0, \quad \omega \in (\omega_h, \infty) \tag{17}$$

Then

$$Q_1 - KQ_2 \approx P_0^{-1}, \quad \omega \in (0, \omega_l) \tag{18}$$

$$K + Q_1 - KQ_2 \approx 0, \quad \omega \in (\omega_h, \infty) \tag{19}$$

1. If the nominal inverse model $P_0^{-1}(s)$ exists and is stable, then, when $\omega \in (0, \omega_l)$, $Q_1 \approx P_0^{-1}$ and $Q_2 \approx 0$, and when $\omega \in (\omega_h, \infty)$, $Q_1 \approx 0$ and $Q_2 \approx 1$. Substitution to equation (9) we get

$$y(j\omega) \approx \frac{P_0K}{1 + P_0K} r(j\omega), \quad \omega \in (0, \omega_l) \tag{20}$$

$$y(j\omega) \approx 0, \quad \omega \in (\omega_h, \infty) \tag{21}$$

Therefore, when the inverse model of the nominal model exists and is stable, the IVDOB not only ensures the good tracking performance of the system but also compensates for the low-frequency disturbance d of the system. Compared with equations (21) and (14), the noise disturbance ξ is also well suppressed.

2. If the nominal inverse model $P_0^{-1}(s)$ does not exist or is unstable, an approximate optimization problem of the model must be considered: $\inf_{Q_3 \in \mathrm{RH}_\infty} \| W_N(I - P_0Q_3) \|_{\infty,2}$. The weight function W_N should be chosen with a high gain when Q_3 is approximated to the inverse of $P_0(s)$. Thus, we have $Q_1 \approx Q_3$ and $Q_2 \approx 0$ when $\omega \in (0, \omega_l)$; $Q_1 \approx 0$ and $Q_2 \approx 1$ when $\omega \in (\omega_h, \infty)$. Similarly, we get the same input–output relation which can be described by equations (10) and (11).

If there is an error in the nominal model $P_0(s)$, the set of the model error can be expressed by additive perturbation. That is, $P_0(s) = P(s) + W_1\Delta$. Here, the weighted function W_1 is bounded and stable with $P(s)$ and $\Delta(s)$ being strictly rational stable functions. Based on the robust stability theory, the necessary and sufficient condition for the IVDOB robust stability can be described as

$$\left\| \frac{1}{(Q_1 + KQ_2)W_1} \right\|_\infty < 1 \tag{22}$$

Theorem 1. As shown in Figure 2, if $P_0(s) \in \mathbf{H}_\infty$, the controller $K(s)$ satisfies the stability requirements of

the closed-loop transfer function and satisfies $Q_1P_0 + Q_2 = 1$. Then, the output of the closed-loop transfer function between the reference input r and the controller $K(s)$ is always the same, namely $G_{ur}(s) = (1 + KP_0)^{-1}K$.

Proof. In Figure 2, when the external disturbance and noise disturbance exist, the following relationships can be obtained

$$\bar{u} = u + Q_1[P_0\bar{u} - (Pd + P\bar{u} + \xi)]$$
$$f = Q_2[P_0\bar{u} - (Pd + P\bar{u} + \xi)] + Pd + P\bar{u} + P\xi$$

Then, we can obtain

$$\bar{u} = \frac{u - Q_1(Pd + \xi)}{1 - Q_1P_0 + Q_1P}$$
$$f = \frac{Q_1P_0 + (1 - Q_2)P}{1 - Q_1P_0 + Q_1P}u - \frac{1 - Q_1P_0 - Q_2}{1 - Q_1P_0 + Q_1P}(Pd + \xi)$$

In addition, $Q_1P_0 + Q_2 = 1$, then $f = P_0u$. Consequently, $G_{ur}(s) = (1 + KP_0)^{-1}K$ and Theorem 1 is proved.

The adaptive fuzzy control system based on the IVDOB

The control structure based on the IVDOB can compensate for the disturbance of the system and realize the control of airborne platform stabilization. The DOB control method, however, cannot fully compensate for all disturbances. Miller and Hilkert[23] state that even though, in different flight conditions, the mUAV has the advantages of small size, lightweight, multi-rotor motor, and so on, there are many unknown nonlinear disturbances in the flight operation process. Due to the existence of these disturbances, the stabilization and tracking performance of the AOEP are affected.

In view of the above analysis, this paper uses the universal approximation property of fuzzy systems to estimate and further compensate the nonlinear unknown disturbance online. An adaptive fuzzy control system based on the IVDOB is designed for improving the stabilization accuracy and tracking performance of AOEPs. The control structure of the adaptive fuzzy control system based on the IVDOB is shown in Figure 3. A double closed-loop structure is adopted. The speed loop is realized by the IVDOB and the position loop is composed of four parts: a PD controller, a feedforward controller, a fuzzy controller, and a robust controller.

Designing the system control law

The fuzzy system is a mapping from $U \in \mathbf{R}^2$ to $\mathbf{R}$, where $U = U_1 \times U_2$, $U_i \subset \mathbf{R}^2$, and $i = 1, 2$. The fuzzy rules are defined as: $\mathbf{R}^{(j)}$: if θ_1 is A_1^j and θ_2 is A_2^j, then u_f is B^j, where the input of the fuzzy system is

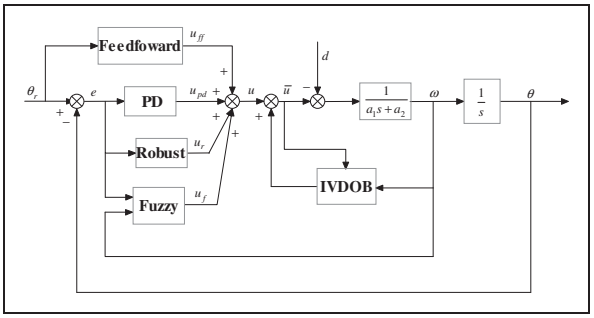

Figure 3. The control structure of an adaptive fuzzy control system based on the IVDOB.

$\underline{\theta} = (\theta_1, \theta_2) = (\theta, \dot{\theta}) \in U$. The output of the fuzzy system is $u_f \in \mathbf{R}$. A_1^j and A_2^j are fuzzy sets on set U_i. $B^j$is a fuzzy set on $\mathbf{R}$, $j = 1, 2 \cdots N$. According to the above rules, the fuzzy system realizes the mapping from the fuzzy set $U \in \mathbf{R}^2$ to $\mathbf{R}$.

Lemma 1.[35] a fuzzy inference system based on single-valued fuzzy logic, product inference engine, and average defuzzification, contains all the functions in the following form

$$u_f(\underline{\theta}) = \frac{\sum_{j=1}^{N} \bar{u}_f^j \left[\prod_{i=1}^{2} \mu_{A_i^j}(\theta_i)\right]}{\sum_{j=1}^{N} \left[\prod_{i=1}^{2} \mu_{A_i^j}(\theta_i)\right]} \tag{23}$$

where $\mu_{B^j}(\bar{u}_f^j)$ is the membership function and $\bar{u}_f^j$ is the maximum value of $\mu_{B^j}(\bar{u}_f^j)$ corresponding to the abscissa function value.

We then introduce the fuzzy basis vector $\underline{\zeta}(\underline{\theta}) = [\zeta_1(\theta_1), \ldots, \zeta_N(\theta_N)]^{\mathrm{T}}$, where $\zeta_j(\underline{\theta}) = \frac{\left[\prod_{i=1}^{2} \mu_{A_i^j}(\theta_i)\right]}{\sum_{j=1}^{N} \left[\prod_{i=1}^{2} \mu_{A_i^j}(\theta_i)\right]}$. The output of the fuzzy system can then be described as

$$u_f(\underline{\theta}) = \underline{\hat{\psi}}^{\mathrm{T}} \underline{\zeta}(\underline{\theta}) \tag{24}$$

where $\underline{\psi} = \left[\bar{u}_f^1, \bar{u}_f^2, \ldots, \bar{u}_f^M\right]^{\mathrm{T}}$ and $\underline{\psi}$ is unknown, commonly used to express the estimated value $\underline{\hat{\psi}}$.

We define position tracking error as

$$e = \theta_r - \theta \tag{25}$$

where θ_r is the given position and θ is the actual position.

According to Figure 3, the control law is obtained as

$$u = u_{ff} + u_{pd} + u_r + u_f \tag{26}$$

where u_{pd}, u_{ff}, u_r and u_f are the output of PD controller, the feedforward controller, the robust controller, and the fuzzy controller, respectively.

The output of the PD controller is

$$u_{pd} = k_{\mathrm{p}}e + k_{\mathrm{d}}\dot{e} \tag{27}$$

The output of the feedforward controller is

$$u_{ff} = \hat{a}_1\ddot{\theta}_r + \hat{a}_2\dot{\theta}_r \tag{28}$$

The output of the fuzzy controller is

$$u_f = \hat{\underline{\psi}}^{\mathrm{T}}\underline{\zeta}(\underline{\theta}) \tag{29}$$

The robust controller is defined in the 'Stability analysis of the control system' section.

Based on equation (10), we know that the control law can be described as

$$\begin{aligned}&\hat{a}_1\ddot{\theta} + \hat{a}_2\dot{\theta} + f(\theta,\dot{\theta},\ddot{\theta})\\ &\quad = \hat{a}_1\ddot{\theta}_r + \hat{a}_2\dot{\theta}_r + k_{\mathrm{p}}e + k_{\mathrm{d}}\dot{e} + \hat{\underline{\psi}}^{\mathrm{T}}\underline{\zeta}(\underline{\theta}) + u_r\end{aligned} \tag{30}$$

That is

$$-[\hat{a}_1\ddot{e} + (\hat{a}_2 + k_{\mathrm{d}})\dot{e} + k_{\mathrm{p}}e] + f(\theta,\dot{\theta},\ddot{\theta}) = \hat{\underline{\psi}}^{\mathrm{T}}\underline{\zeta}(\underline{\theta}) + u_r \tag{31}$$

In this paper, the fuzzy controller is used to compensate for the unknown disturbance by using the universal approximation property of fuzzy systems. Therefore, we have $f(\theta,\dot{\theta},\ddot{\theta}) = \underline{\psi}^{*\mathrm{T}}\underline{\zeta}(\underline{\theta}) + \delta$, where $\underline{\psi}^* = \min_{\underline{\psi}\in\Omega_{\underline{\psi}}}[\sup_{\underline{\theta}\in\Omega_{\underline{\theta}}}\|f(\theta,\dot{\theta},\ddot{\theta}). - \underline{\psi}^{\mathrm{T}}\underline{\zeta}(\underline{\theta})\|]$ is the optimal estimated value of $\underline{\psi}$ and δ is the approximation error, where $|\delta| < \varphi$, $\varphi > 0$. The estimated value of $\underline{\psi}$ and φ exist and the estimation error is $\tilde{\underline{\psi}} = \underline{\psi}^* - \hat{\underline{\psi}}$ and $\tilde{\varphi} = \varphi - \hat{\varphi}$, where $\hat{\underline{\psi}}$ is the estimated value of $\underline{\psi}$ and $\hat{\varphi}$ is the estimated value of φ.

We get

$$\hat{a}_1\ddot{e} + (\hat{a}_2 + k_{\mathrm{d}})\dot{e} + k_{\mathrm{p}}e = \tilde{\underline{\psi}}^{\mathrm{T}}\underline{\zeta}(\underline{\theta}) + \delta - u_r \tag{32}$$

Letting $\mathbf{X} = \begin{bmatrix} e \\ \dot{e} \end{bmatrix}$, $\mathbf{A} = \begin{bmatrix} 0 & 1 \\ -\frac{k_{\mathrm{p}}}{\hat{a}_1} & -\frac{\hat{a}_2 + k_{\mathrm{d}}}{\hat{a}_1} \end{bmatrix}$, $\mathbf{B} = \begin{bmatrix} 0 \\ \frac{1}{\hat{a}_1} \end{bmatrix}$, $\mathbf{\Delta} = \tilde{\underline{\psi}}^{\mathrm{T}}\underline{\zeta}(\underline{\theta}) + \delta - u_r$, the state space of the system control law is obtained by

$$\dot{\mathbf{X}} = \mathbf{A}\mathbf{X} + \mathbf{B}\mathbf{\Delta} \tag{33}$$

Stability analysis of the control system

Due to the asymptotic stability of matrix $\boldsymbol{A}$, for any positive definite symmetric matrix $\boldsymbol{Q}$, only the positive definite symmetric matrix $\mathbf{P}$ makes the establishment of the Lyapunov equation.

The Lyapunov function is defined as follows

$$V = \frac{1}{2}\mathbf{X}^{\mathrm{T}}\mathbf{P}\mathbf{X} + \frac{1}{2\gamma_1}tr(\tilde{\underline{\psi}}^{\mathrm{T}}\tilde{\underline{\psi}}) + \frac{1}{2\gamma_2}\tilde{\varphi}^2 \tag{34}$$

where γ_1 and γ_2 are the learning coefficients; $\gamma_1 > 0$ and $\gamma_2 > 0$. The derivative of equation (34) is

$$\begin{aligned}\dot{V} = &\frac{1}{2}\mathbf{X}^{\mathrm{T}}(\mathbf{A}^{\mathrm{T}}\mathbf{P} + \mathbf{P}\mathbf{A})\mathbf{X} + \mathbf{\Delta}^{\mathrm{T}}\mathbf{B}^{\mathrm{T}}\mathbf{P}\mathbf{X} + \frac{1}{\gamma_1}tr(\tilde{\underline{\psi}}^{\mathrm{T}}\dot{\tilde{\underline{\psi}}})\\ &+ \frac{1}{\gamma_2}\tilde{\varphi}\dot{\tilde{\varphi}}\end{aligned} \tag{35}$$

where $\mathbf{A}^{\mathrm{T}}\mathbf{P} + \mathbf{P}\mathbf{A} = -\mathbf{Q}$, where $\mathbf{P}$ and $\mathbf{Q}$ are positive definite symmetric matrices.

Letting $\mathbf{P} = \begin{bmatrix} p_{11} & p_{12} \\ p_{21} & p_{22} \end{bmatrix}$, $\lambda = \frac{p_{22}}{\hat{a}_1}\dot{e} + \frac{p_{21}}{\hat{a}_1}e$, then $\mathbf{\Delta}^{\mathrm{T}}\mathbf{B}^{\mathrm{T}}\mathbf{P}\mathbf{X} = \mathbf{\Delta}\lambda$ and equation (35) can be simplified as

$$\begin{aligned}\dot{V} = &-\frac{1}{2}\mathbf{X}^{\mathrm{T}}\mathbf{Q}\mathbf{X} + \tilde{\underline{\psi}}^{\mathrm{T}}\underline{\zeta}(\underline{\theta})\lambda + \delta\lambda - u_r\lambda - \frac{1}{\gamma_1}\tilde{\underline{\psi}}^{\mathrm{T}}\dot{\underline{\psi}}\\ &+ \frac{1}{\gamma_2}\hat{\varphi}\dot{\hat{\varphi}} - \frac{1}{\gamma_2}\varphi\dot{\hat{\varphi}}\end{aligned} \tag{36}$$

Let

$$\dot{\hat{\underline{\psi}}} = \gamma_1\lambda\underline{\zeta}(\underline{\theta}) \tag{37}$$

$$\dot{\hat{\varphi}} = \gamma_2 \cdot \lambda \cdot \mathrm{sgn}(\lambda) \tag{38}$$

$$u_r = \hat{\varphi} \cdot \mathrm{sgn}(\lambda) \tag{39}$$

By substituting equations (37) to (39) into equation (36), we have

$$\dot{V} = -\frac{1}{2}\mathbf{X}^{\mathrm{T}}\mathbf{Q}\mathbf{X} + \delta\lambda - \varphi|\lambda| \leqslant -\frac{1}{2}\mathbf{X}^{\mathrm{T}}\mathbf{Q}\mathbf{X} + |\lambda|(|\delta| - \varphi) \tag{40}$$

Figure 4. The stable tracking control system of an AOEP mounted on a Hex-Rotor UAV for experimentation.

where $\mathbf{Q}$ is a positive definite symmetric matrix and $|\delta| < \varphi$. Then we have

$$\dot{V} \leqslant -\frac{1}{2}\mathbf{X}^{\mathrm{T}}\mathbf{Q}\mathbf{X} < 0 \tag{41}$$

Theorem 2. The system model is shown in equation (11), when the control law shown in equations (26) to (29), and (39) was adopted and the parameter adaptive law shown in equations (37) and (38) was used. In the presence of disturbance, the system asymptotically stabilizes and the tracking error becomes bounded and asymptotically converges to zero.

Table 1. Physical parameters of the Hex-Rotor UAV.

Physical parameters	Values
Takeoff weight	7.5 (kg)
Empty weight(battery not include)	3.95 (kg)
Battery capacity	10,000 (mAh)
Number of DC motors	6
Number of rotors	12
Time of flight	25 (min)
Working temperature	−30°C to 40°C

Table 2. Parameters of the airborne platform system.

Parameters of AOEP	Values
Pitch channel, M_e	0.0314 (kg·m^2)
Pitch channel, F_V	0.0023 (N·ms/rad)
Yaw channel, M_e	0.4286 (kg·m^2)
Yaw channel, F_V	0.0055 (N·ms/rad)
Parameters, $\hat{a}_1$	0.5
Parameters, $\hat{a}_2$	2

Proof. According to the Lyapunov direct method, we know that the tracking error e, the parameter estimation error $\underline{\tilde{\psi}}$, and $\tilde{\varphi}$ are globally uniformly bounded. $\underline{\psi}$, φ are unknown normal numbers where $\underline{\tilde{\psi}} = \underline{\psi}^* - \underline{\hat{\psi}}$ and $\tilde{\varphi} = \varphi - \hat{\varphi}$. Therefore, the estimated values $\underline{\hat{\psi}}$ and $\hat{\varphi}$ are also globally uniformly bounded. In addition, the given position θ_r is bounded, according to equation (21). It also shows that θ is globally uniformly bounded and that the velocity output ω is also bounded. According to equations (26) to (29) and (39), it is shown that u_{ff}, u_{pd}, u_r and u_f are bounded. Then the output u is also bounded. Thus, it is proven that all the signals in the system are bounded.

In addition, according to equations (40) and (41), $e \in L_2$ and $\dot{e} \in L_2$. Therefore, $e \to 0$ while $t \to \infty$. Thus, Theorem 2 is proved.

Experimental studies

In this experiment, the stable tracking control system of an AOEP mounted on a Hex-Rotor UAV is taken as the research object, as shown in Figure 4. The physical parameters of the mUAV are shown in Table 1.

The system adopts TMS320F28335 as the processor and the whole control period is about 30 ms. The photoelectric encoder is used as the position sensor, and its measurement accuracy is 60″. A certain sensor with an integrated three-axis gyro and three-axis accelerometer is used as the speed sensor and the acceleration sensor. The parameters of the AOEP model are identified by the sweep frequency method and shown in Table 2.

The setting of the parameters of the control system is as follows:

1. For the IVDOB, selecting the typical $Q_{31}(s)$ filter as the low pass filter $Q_1(s)$ with a time constant of

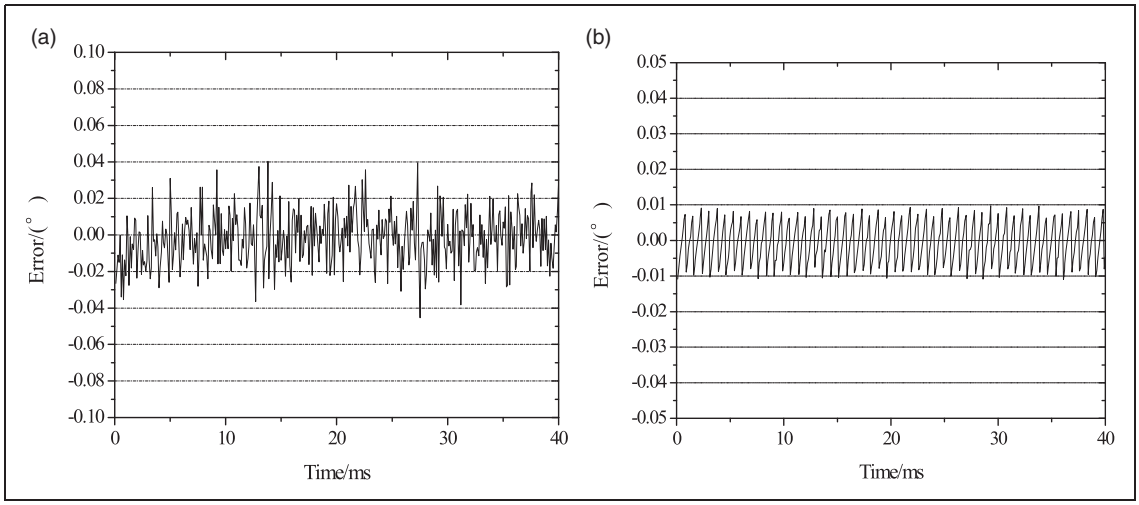

Figure 5. The comparison results of the LOS angle error: (a) the angle error with VDOB; (b) the angle error with IVDOB.

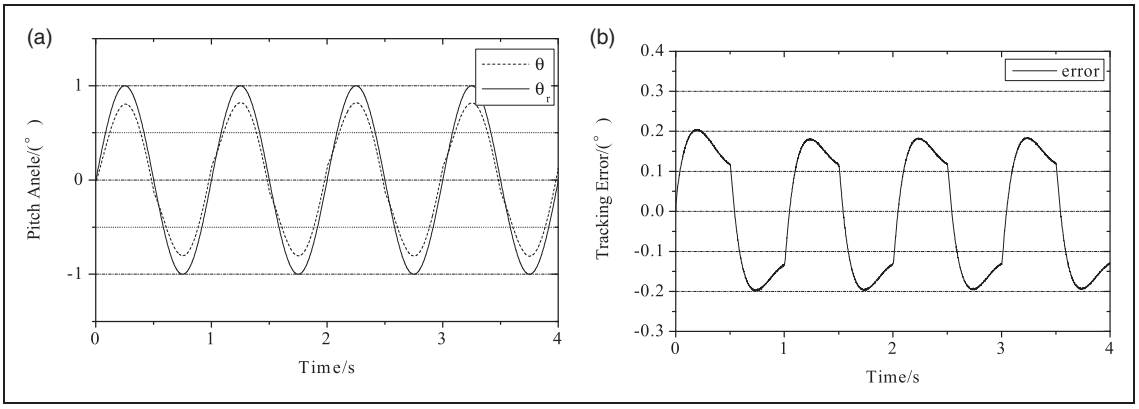

Figure 6. The tracking curve and tracking error without the fuzzy self-adjusting controller: (a) the position tracking curve; (b) the tracking error.

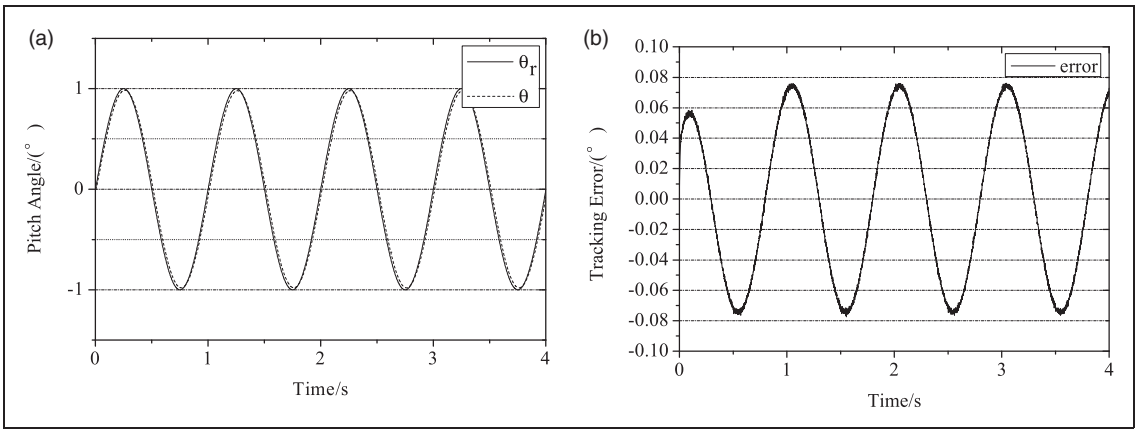

Figure 7. The tracking curve and tracking error with the fuzzy self-adjusting controller: (a) the position tracking curve; (b) the tracking error.

Figure 8. Flight experiment of the proposed control system.

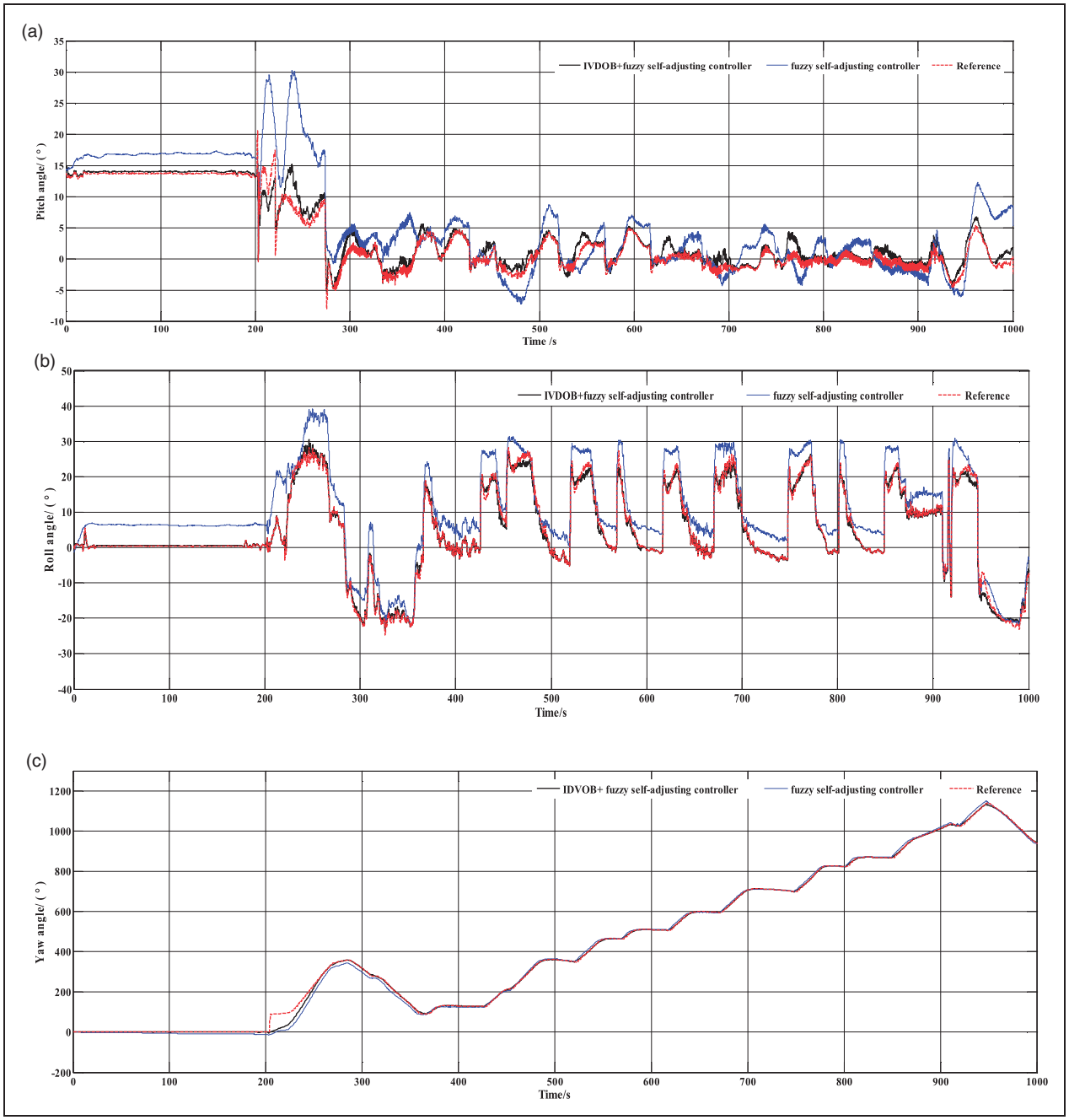

Figure 9. Comparison of tracking curves of the proposed controller and the fuzzy self-adjusting controller (a) pitch channel; (b) roll channel; (c) yaw channel.

$\tau = 0.001$s, the low pass filter is given by

$$Q_1(s) = \frac{3\tau s + 1}{\tau^3 s^3 + 3\tau^2 s^2 + 3\tau s + 1}$$

By Theorem 1

$Q_2(s) = 1 - P(s)Q_1(s) = 1 - [\mathbf{C}(s\mathbf{I} - \mathbf{A})^{-1}\mathbf{B}]Q_1(s)$. Then $\mathbf{A}$, $\mathbf{B}$, and $\mathbf{C}$ in equation (9) are substituted into $Q_2(s)$ and we get

$$Q_2(s) = 1 - 31.847\frac{1}{s(s-0.732)}\frac{3\tau s + 1}{\tau^3 s^3 + 3\tau^2 s^2 + 3\tau s + 1}$$

2. The PD controller parameters is obtained by Z-N method: $k_p = 15.0035$, $k_d = 1.9961$.
3. The positive definite symmetric matrix: $\mathbf{Q} = \begin{bmatrix} 1000 & 200 \\ 200 & 100 \end{bmatrix}$.
4. The learning coefficients: $\gamma_1 = 200$, $\gamma_2 = 0.1$.
5. The fuzzy controller: the membership functions of the fuzzy input angle θ are: $\mu_{A_1^1} = e^{-(\theta+1)^2}$, $\mu_{A_1^2} = e^{-(\theta+0.5)^2}$, $\mu_{A_1^3} = e^{-(\theta+0.0)^2}$, $\mu_{A_1^4} = e^{-(\theta-0.5)^2}$, and $\mu_{A_1^5} = e^{-(\theta-1)^2}$. The membership function of the fuzzy input angular velocity $\dot{\theta}$ are: $\mu_{A_2^1} = e^{-0.5(\theta+8)^2}$, $\mu_{A_2^2} = e^{-0.5(\theta+4)^2}$, $\mu_{A_2^3} = e^{-0.5(\theta+0.0)^2}$, $\mu_{A_2^4} = e^{-0.5(\theta-4)^2}$, and $\mu_{A_2^5} = e^{-0.5(\theta-8)^2}$.

The LOS stabilization control experiment

We used the line of sight (LOS) stabilization control experiment to verify the capability of the proposed IVDOB. The VDOB and IVDOB control structure are designed based on Figures 1 and 2. Taking the pitch channel as an example, the given pitch angle of the AOEP is 0°. Under the condition of two kinds of DOB, the position sensor on the pitch direction is sampled by a sampling frequency of 100 Hz and the actual angle information is acquired.

Figure 5(a) is the LOS angle error curve with the VDOB; the maximum angle error is less than 0.04° and the stability precision is about 0.52 mrad. Figure 5(b) is the LOS angle error curve with the IVDOB; the maximum angle error is less than 0.01° and the stability precision is about 0.13 mrad. The results show that the proposed IVDOB structure has a better disturbance rejection ability and higher accuracy of LOS stabilization.

The tracking experiment of a given position signal

The control system is designed according to Figure 3. We used the experiment of tracking a given position signal to verify the ability of disturbance compensation of the proposed adaptive fuzzy control system based on the IVDOB.

The tracking curve and tracking error without the fuzzy self-adjusting controller are shown in Figure 6. As can be seen from Figure 6, the tracking error reaches 0.2° and it is difficult to achieve accurate tracking of the given signal.

The tracking curve and tracking error with the fuzzy self-adjusting controller are shown in Figure 7. The tracking error is not more than 0.08° and the tracking error is bounded. Obviously, the control method proposed in this paper has a better tracking effect and can accurately track the given position signal.

The stable tracking control system of an AOEP mounted on a Hex-Rotor UAV was tested with wind speed conditions of about 3.2 m/s while the Hex-Rotor UAV is moving, as shown in Figure 8. In order to verify the effectiveness of the proposed method, a comparative experiment with the traditional fuzzy self-adjusting controller is carried out. The results are shown in Figure 9. As can be seen from Figure 9, the traditional fuzzy self-adjusting controller can track the given position in each channel. However, the tracking effect is not ideal, and there are large tracking errors, especially in the case of large angle motion in the pitching and rolling channels. By comparison, the proposed method can track the given position signal accurately, and the tracking error is small.

Conclusions

Theoretical analysis and the experimental results show that the maximum LOS angle error is less than 0.01° and the stability precision is about 0.13 mrad when $Q_2(s)$ is introduced into the IVDOB. Furthermore, the disturbance compensation ability of the IVDOB had improved. The fuzzy adaptive control method can be used to approximate and compensate the unknown nonlinear disturbance of AOEP systems. The tracking error of the given position signal is less, the tracking error is bounded, and the system is asymptotically stable. The proposed method has good stability and robustness. In summary, the control method proposed in this paper can meet the requirements for the AOEP tracking control of mUAVs.

Author contributions

Rijun Wang is the main author, having written the content and conducted the survey. Yue Bai, Zhiqiang Zeng, Junyuan Wang, Wenhua Du and Nengquan Duan has contributed with numerous comments, as well as content in the Introduction and Abstract.

Declaration of Conflicting Interests

The author(s) declared no potential conflicts of interest with respect to the research, authorship, and/or publication of this article.

Funding

The author(s) disclosed receipt of the following financial support for the research, authorship, and/or publication of this article: This study was co-supported by the National Natural Science Foundation of China (Nos 11372309 and 6130401), Natural Science Foundation of Shanxi Province of China (Nos 201801D121187) and the Science Foundation of North University of China (Nos XJJ2016006).

ORCID iD

Rijun Wang http://orcid.org/0000-0003-1576-0793

References

1. Zhang X, Li X, Pei HK, et al. Design of self balancing anti disturbance system for multi rotor UAV. *Telecomm Comput Electron Control* 2016; 14: 363–371.
2. Araar O, Aouf N and Vitanov I. Vision based autonomous landing of multirotor UAV on moving platform. *J Intell Robot Syst* 2016; 85: 369–384.
3. Tang ZF. Advance in rotorcraft technology. Report, Nanjing University of Aeronautics and Astronautics, China, April, 2011.
4. Gao W and Zhu M. Actuality of photoelectricity platform and tracking system for UAV. *Ome Information* 2011; 28: 33–40.
5. Windau J and Itti L. Multilayer real-time video image stabilization. In: *IEEE/RJS international conference on intelligent robots and systems*, San Francisco, USA, 25–30 September 2011, pp.2397–2402. New York: IEEE.

6. Eisenbeiss H. A mini unmanned aerial vehicle (UAV): system overview and image acquisition. In: *International workshop on processing and visualization using high-resolution imagery*, Pitsanulok, Thailand, 18–20 November 2004, pp.10–16. Nice: ISPRS.
7. Umeno T, Kaneko T and Hori Y. Robust servo system design with two degrees of freedom and its application to novel motion control of robot manipulators. *IEEE Trans Ind Electron* 1993; 40: 473–485.
8. Chen WH, Yang J, Guo L, et al. Disturbance observer-based control and related methods: an overview. *IEEE Trans Ind Electron* 2016; 63: 1083–1095.
9. Chen SL, Shan ML and Wang LB. Disturbance observer-based robust perfect tracking control for flight simulator. *Electr Mach Control* 2015; 19: 113–118.
10. Wang RJ, Bai Y, Xu ZJ, et al. A composite disturbance compensation method for airborne platform based on improved disturbance observer. *J Optoelectron·Laser* 2015; 26: 108–115.
11. Wei W, Dai M, Li JQ, et al. Design of the disturbance observer of opto-electronic platform in frequency domain. *J Shandong Univ (Eng Sci)* 2015; 45: 45–49.
12. Zhu HR, Li Q, Fang SX, et al. Disturbance observer based compound control of inertially stabilized platform. *J Nanjing Univ Sci Technol (Nat Sci)* 2009; 33: 263–268.
13. Man HL, Park HG, Lee WB, et al. On the design of a disturbance observer for moving target tracking of an autonomous surveillance robot. *Int J Control Autom Syst* 2012; 10: 117–125.
14. Kempfc J and Kobayashi S. Disturbance observer and feed forward design for a high-speed direct-drive positioning table. *IEEE Trans Control Syst Technol* 1999; 7: 513–526.
15. Xie W and He ZL. Control method with improved disturbance observer. *Control Theory Appl* 2010; 27: 695–700.
16. Ji KH and Shen JX. A low speed motor drive system with disturbance torque observer. *Proc CSEE* 2012; 32: 100–106.
17. Lee KB. Disturbance observer that use radial basis function networks for the low speed control of a servo motor. *IEE Proc – Control Theory Appl* 2005; 152: 526–536.
18. Wei W, Li XY, Zuo M, et al. Parameter tuning rule for velocity based disturbance observer. *Comput Simul* 2014; 31: 372–376.
19. Li JQ, Ding C, Kong DJ, et al. Velocity based disturbance observer and its application to photoelectric stabilized platform. *Optics Prec Eng* 2011; 19: 998–1004.
20. Li SS, Zhong NY and Zhao Y. Estimation and compensation of unknown disturbance in three-axis gyro-stabilized camera mount. *Trans Inst Meas Control* 2015; 37: 732–745.
21. Wang YY, Dai M, Ding C, et al. Application of high order observer in EO stabilized platform. *Optics Prec Eng* 2015; 23: 459–466.
22. Fuwa K, Narikiyo T, Kandoh H, et al. A construction of disturbance observer to cope with frequency variation and its application to vibration suppression control system. *IFC Proc Vol* 2008; 41: 2696–2701.
23. Miller R and Hilkert JM. Gimbal system configurations and line-of-sight control techniques for small UAV applications. In: *Airborne intelligence, surveillance, reconnaissance (ISR) systems and applications X*, 871308. Baltimore, Maryland, USA, 31 May 2013, pp.1–15. Washington: SPIE.
24. Mudi RK and Pal NR. A robust self-tuning scheme for PI- and PD-type fuzzy controllers. *IEEE Trans Fuzzy Syst* 1999; 7: 2–16.
25. Ji W and Li Q. Adaptive fuzzy PID control for LOS stabilization system on gyro stabilized platform. *Acta Aeronaut Astronaut Sin* 2007; 28: 191–195.
26. Fang J and Yin R. An adaptive nonlinear control for gyro stabilized platform based on neural networks and disturbance observer. *Math Prob Eng*. Epub ahead of print 2014. DOI: 10.1155/2014/472815.
27. Ji W, Li Q, Xu B, et al. Adaptive fuzzy PID composite control with hysteresis-band switching for line of sight stabilization servo system. *Aerosp Sci Technol* 2011; 15: 25–32.
28. Lei X, Zou Y and Dong F. A composite control method based on the adaptive RBFNN feedback control and the ESO for two-axis inertially stabilized platforms. *ISA Trans* 2015; 59: 424–433.
29. Wang M, Zhang H, Wang XF, et al. A novel servo control method based on feedforward control-Fuzzy-grey predictive controller for stabilized and tracking platform system. *J Vibroeng* 2016; 18: 5266–5280.
30. Wang RJ, Bai Y, Xu ZJ, et al. Fuzzy self-adjusting tracking control based on disturbance observer for airborne platform mounted on multi-rotor unmanned aerial vehicle. *J Zhejiang Univ (Eng Sci)* 2015; 49: 2005–2012.
31. Fang J, Yin R and Lei X. An adaptive decoupling control for three-axis gyro stabilized platform based on neural networks. *Mechatronics* 2015; 27: 38–46.
32. Hu HJ, Yue JY and Zhang P. A control scheme based on RBF neural network for high-precision servo system. In: *International conference on mechatronics and automation*, Xi'an, China, 4–7 August 2010, pp.1489–1494. New York: IEEE.
33. Khalil HK. *Nonlinear system*. 3rd ed. New Jersey: Prentice Hall, 2002, pp.24–25.
34. Sarwai IS and Malik AM. Modeling, analysis and simulation of a Pan tilt platform based on linear and nonlinear systems. In: *IEEE/ASME International Conference on Mechtronic and Embedded Systems and Applications*, Beijing, China, 12–15 October 2008, pp.147–152. New York: IEEE.
35. Jin-Kun L. *Advanced PID control and Matlab simulation*. 4th ed. Beijing: Electronic Industry Press, 2016, pp.285–295.